

Proposal to Jefferson Lab PAC 17

A CLEAN MEASUREMENT OF THE NEUTRON SKIN OF  $^{208}\text{Pb}$   
THROUGH PARITY VIOLATING ELECTRON SCATTERING

Spokesmen: R. Michaels, P.A. Souder, G.M. Urciuoli

K.A. Aniol, M.B. Epstein, D.J. Margaziotis  
*California State Univerisity, Los Angeles*

P.A. Souder, R. Holmes  
*Syracuse University*

E. Burtin, C. Cavata, B. Frois, D. Lhuillier, F. Marie, T. Pussieux  
*DSM/DAPNIA/SPhN CEA Saclay*

R. Carlini, J.P. Chen, E. Chudakov, K. De Jager, J. Gomez, M. Kuss, J. LeRose,  
M. Liang, R. Michaels, J. Mitchell, A. Saha, B. Wojtsekhowski  
*Thomas Jefferson National Accelerator Facility*

M. Amarian, E. Cisbani, S. Frullani, F. Garibaldi, M. Iodice,  
R. Iommi, G.M. Urciuoli  
*INFN/Rome*

R. De Leo  
*INFN/Bari*

R. Wilson  
*Harvard University*

(over)

C.J. Horowitz  
*Indiana University*

G.D. Cates, B. Humensky  
*Princeton University*

K. Kumar  
*University of Massachusetts*

P. Markowitz  
*Florida International University*

J. Calarco, W. Hersman  
*University of New Hampshire*

J.M. Finn, T. Averett, D. Armstrong  
*College of William and Mary in Virginia*

*(This is a Hall A Collaboration Proposal)*

Postscript copy of this proposal is at [www.jlab.org/~rom/pbpro.ps](http://www.jlab.org/~rom/pbpro.ps)

## ABSTRACT

The difference between the neutron radius  $R_n$  of a heavy nucleus and the proton radius  $R_p$  is believed to be on the order of several percent. This qualitative feature of nuclei, which is essentially a neutron skin, has proven to be elusive to pin down experimentally in a rigorous fashion. We propose to measure the parity-violating electroweak asymmetry in the elastic scattering of polarized electrons from  $^{208}\text{Pb}$  at an energy of 850 MeV and a scattering angle of  $6^\circ$ . Since the  $Z_0$  boson couples mainly to neutrons, this asymmetry provides a measure of the size of  $R_n$  with respect to  $R_p$  that can be interpreted with as much confidence as traditional electron scattering data. The projected experimental precision corresponds to a  $\pm 1\%$  determination of  $R_n$ , which will access the range of values predicted by nuclear theory, thus establishing the existence of the neutron skin if it is of the expected size.

# A Clean Measurement of the Neutron Skin of $^{208}\text{Pb}$ Through Parity Violating Electron Scattering

## I INTRODUCTION

The neutron radius  $R_n$  in  $^{208}\text{Pb}$  is generally assumed to be about 0.25 fm larger than the proton radius  $R_p \sim 5.5$  fm. This “neutron skin” is a fundamental qualitative feature of nuclear structure characteristic of large nuclei that has never been cleanly observed in a stable nucleus.

The proton radius of the nucleus can be cleanly measured by, for example, electron scattering or the spectroscopy of muonic atoms [1]. Determining the neutron radius of the nucleus is more complex. Electron scattering from neutrons is primarily magnetic and thus does not directly measure the neutron density because most of the neutrons in a heavy nucleus couple to spin zero. Hence hadronic probes such as pions and protons must be used, and the interpretation of the data has serious theoretical difficulties at the desired level of precision. Our opinion, based on private conversations and reading the literature, is that the uncertainty in the neutron radius is at present 5%, if not larger. We feel that it is extremely important to reduce this error to the 1% level so that we can definitively state whether or not this feature of nuclei exists. This experiment has the potential to be a benchmark for nuclear physics in the same way that charge density measurements established our picture of the size and shapes of nuclei about 15 years ago. The single measurement proposed here will have implications in atomic, nuclear, and astrophysics.

One possible clean way to measure the neutron skin is to use the weak interaction. In the Standard Model, the proton coupling to the Z-boson is much smaller than that of the neutron due to an accidental cancellation. A measurement of the weak neutral current amplitude in elastic electron scattering can be used to measure the neutron radius with the same level of confidence that electromagnetic probes determine  $R_p$ . Some time ago, it was pointed out that parity-violation in the elastic scattering of polarized electrons is a practical method for using the Z-boson to determine neutron radii [2]. Recently, a realistic calculation of the asymmetries, taking into account the distortion of the electron wavefunctions, has been published [3].

Based on the results of Ref. [3], we have designed an experiment to measure  $R_n$ . It requires measuring the parity-violating amplitude in elastic  $\vec{e}-^{208}\text{Pb}$

scattering at the 3% level. The experiment will be sensitive to the  $R_n$  at the 1% level, ample to establish presence of the neutron skin.

## II THEORY

### A Knowledge of Neutron Radii

The “neutron skin” is potentially a fundamental feature of heavy nuclei. The important question that we address here is exactly what empirical basis we have at present for accepting the existence of this feature. The most detailed published discussion of this issue, by Pollock, Fortson, and Wilets (PFW) [4], was written in the somewhat interdisciplinary context of using parity violation in heavy atoms as a test of the Standard Model. It turns out that the answer is not simple. The information on the neutron radius is somewhat indirect, comes from many sources, and depends on theoretical input with uncertainties that are hard to pin down. As a result, there are not many published estimates of the total error in  $R_n$ . A paper by Fortson *et al.* [5] suggests  $\delta R_n \sim 10\%$ . There are probably also experts in the field that would quote an error at the level of 3% or less.

To illustrate some of the issues, we will briefly review how  $R_n$  is determined, following the discussion of PFW. One source of information comes from Hartree-Fock calculations based on phenomenological potentials that reproduce a large body of data. The main goal of our experiment is to constrain these effective interactions. A summary of relevant calculations as given by PFW is reproduced in table 1 for  $^{208}\text{Pb}$ .

	$R_n/R_p$	$q_n$
G:HFB	1.025	0.90260
SkA	1.039	0.90051
Sk*	1.031	0.90176
Sk3	1.023	0.90334
Rel	1.056	0.89813

**TABLE 1.** Comparison of Hartree-Fock Calculations of  $R_n$  for  $^{208}\text{Pb}$ . Also shown is the quantity  $q_n$ , a parameter in the computation of atomic parity violation.

The spread in the calculations of  $R_n/R_p$  is seen to be 0.03. The relevant question is *how much can  $R_n/R_p$  be changed without losing the successes of the*

*calculation* ? There is no published answer to this question, but accommodating changes in  $R_n/R_p$  of 0.05 or more is plausible [5]. We conclude that the Hartree-Fock calculations, even with their many successes, do not conclusively establish the existence of the neutron skin.

Another quantitative estimate of the thickness of the neutron skin appears in a paper on scattering experiments. The result, using data on the scattering of polarized protons from  $^{208}\text{Pb}$ , is an impressive value  $R_n - R_p = 0.14 \pm 0.04$  fm (relative to  $R_p \sim 5.45$  fm) [6]. However, PFW states that there are additional theoretical uncertainties arising from the hadronic nature of the proton as a probe that add considerable error. Moreover, the value for  $R_n - R_p$  exhibits a large and unphysical dependence on the energy of the beam used for the experiment [6] as shown in Fig. 1.

Data comparing the elastic scattering of positive and negative pions exist [7], but again there are uncertainties in the analysis [4]. These methods are not really directly sensitive to the neutron distribution.

The method of using parity violation described in this proposal is directly sensitive to the neutron radius. The uncertainties in the theoretical interpretation of the results (discussed in more detail below) are expected to be much smaller than the problems just discussed. If we can achieve our projected experimental error and if the neutron skin is of the expected thickness, we can cleanly establish its existence.

## B Summary of Physics Motivation

Based on the discussion of our understanding of the neutron skin stated above, we are motivated to do our experiment for the following reasons:

1. Establish and characterize the neutron skin. This is a striking feature of heavy stable nuclei which has not been definitely established.
2. Accurate neutron density measurements have a broad impact on nuclear physics, in particular neutron structure, isovector interactions, the structure of neutron-rich radioactive beams, and neutron-rich matter in astrophysics [3] [8]. This measurement will be a calibration point for nuclear theory, as is illustrated in figure 2 (taken from ref [9]).
3. Constrain neutron densities for atomic PNC experiments. In the future the most precise low energy test of the Standard Model may involve the combination of this, or follow-on, neutron density experiments to constrain the nuclear structure in an atomic PNC measurement.

These physics issues and the opportunity represented by this proposal have motivated a workshop on “Parity Violation in Atomic, Nuclear, and Hadronic Systems” which will be held June 5–16, 2000 in Trento, Italy. This has been approved and majority funded by the ECT\*.

## C Parity Violation in Heavy Atoms

The neutron radius is also important for precise studies of parity violation in atomic physics. The reason is as follows. The solution of the Dirac equation for the naive potential of uniform charge density for  $r < R$

$$V(r) = Ze^2 \times \begin{cases} (-3 + r^2/R^2)/2R & r < R, \\ -1/r & r > R. \end{cases} \quad (1)$$

normalized to unity at the origin, is

$$f(r) = 1 - \frac{1}{2}(Z\alpha)^2 \left[ \left(\frac{r}{R}\right)^2 - \frac{1}{5}\left(\frac{r}{R}\right)^4 + \frac{1}{75}\left(\frac{r}{R}\right)^6 \right] \quad (2)$$

At the surface,  $f(r)$  has changed by  $\sim 20\%$ . The average of  $f(r)$  is

$$q_n = \int \rho_n(r) f(r) d^3r \sim 1 - \frac{3}{70}(Z\alpha)[1 + 5R_n^2/R_p^2] \sim 0.9 \quad (3)$$

as shown in Table 1 for  $^{208}\text{Pb}$ . Here  $R_{p(n)}$  is the proton(neutron) radius. The difference between  $q_n$  and unity is approximately proportional to  $(R_n/R_p)^2$  under the assumption that the neutron density is approximately constant and if  $R_n \sim R_p$ . Without these assumptions, more information about the shape of the neutron density is needed. However, the values for  $q_n$  shown above in Table 1 for all the calculations are linearly related, suggesting that measuring a single parameter is sufficient at the needed level of precision.

The atomic parity-violating amplitudes are approximately proportional to  $q_n$ . The experimental error in the atomic experiment on Cs is presently at the 0.3% level. The atomic theory is uncertain at the 1% level, which is larger than the error in  $q_n$ . However, extensive work is underway to improve the atomic physics experiments using a variety of new techniques. The atomic calculations are expected to be feasible at the required level of precision. Hence, we believe that our measurement of  $R_n$  will become important to this field.

## D Parity-Violation and the Neutron Radius

The potential between an electron and a nucleus may be written

$$\hat{V}(r) = V(r) + \gamma_5 A(r) \quad (4)$$

where the usual electromagnetic vector potential is

$$V(r) = \int d^3r' Z\rho(r')/|\vec{r} - \vec{r}'| \quad (5)$$

and where the charge density  $\rho(r)$  is closely related to the point proton density  $\rho_p(r)$  given by

$$Z\rho_p(r) = \sum_p \langle \psi_p^\dagger(r) \psi_p(r) \rangle. \quad (6)$$

The axial potential  $A(r)$  depends also on the neutron density:

$$N\rho_n(r) = \sum_p \langle \psi_n^\dagger(r) \psi_n(r) \rangle. \quad (7)$$

It is given by

$$A(r) = \frac{G_F}{2^{3/2}} [(1 - 4\sin^2\theta_W)Z\rho_p(r) - N\rho_n(r)] \quad (8)$$

The axial potential has two important features:

1. It is much smaller than the vector potential, so it is best observed by measuring parity violation.
2. Since  $\sin^2\theta_W \sim 0.23$ ,  $(1 - 4\sin^2\theta_W)$  is small and  $A(r)$  depends mainly on the neutron radius  $\rho_n(r)$ .

The cross section for scattering electrons with momentum transfer squared  $Q^2$  is given by

$$\frac{d\sigma}{d\Omega} = \frac{d\sigma}{d\Omega_{\text{Mott}}} |F_p(Q^2)|^2 \quad (9)$$

where

$$F_p(Q^2) = \frac{1}{4\pi} \int d^3r j_0(Qr) \rho_p(r) \quad (10)$$

is the form factor for protons.

One can also define a form factor for neutrons

$$F_n(Q^2) = \frac{1}{4\pi} \int d^3r j_0(Qr) \rho_n(r) \quad (11)$$

By scattering polarized electrons, one can measure the parity-violating asymmetry which is the interference term between  $V(r)$  and  $A(r)$

$$A_{LR} = \frac{\sigma_R - \sigma_L}{\sigma_R + \sigma_L}, \quad (12)$$

where  $\sigma_{L(R)}$  is the cross section for the scattering of left(right) handed electrons. The result is

$$A_{LR} = \frac{G_F Q^2}{4\pi\alpha\sqrt{2}} \left[ 1 - 4\sin^2\theta_W - \frac{F_n(Q^2)}{F_p(Q^2)} \right] \quad (13)$$

Thus  $A_{LR}$  is approximately proportional to the ratio of neutron to proton form factors.

## E Realistic Calculations

The above analysis assumes plane waves for the electrons. For heavy nuclei such as Pb, this is a poor approximation. Hence the analysis must be done for scattering states that are solutions to the Dirac Equation

$$[\alpha \cdot \mathbf{p} + \beta m_e + \hat{V}(r)]\psi = E\psi \tag{14}$$

valid when  $Z\alpha$  is relatively large. This has been done by Horowitz [3].

There are three vital questions about the realistic solution:

1. How large are the effects of the distortions on the asymmetries ?
2. How sensitive are the asymmetries to the neutron radius ?
3. How precise are the calculations ?

The distortions are substantial, as shown in Fig. 3, typically on the order of 20%, but vary strongly with  $Q^2$ . At certain values of  $Q^2$  the asymmetries depend strongly on the neutron radius. There is a point below the first diffraction dip where a 3% measurement of  $A_{LR}$  yields the desired 1% measurement of the neutron radius.

The calculations are precise enough to support the experiment and pass several stringent tests as explained in ref [3]. Recently the numerical accuracy has been verified by three independent codes [10].

One important question is how do we measure  $R_n$  with a measurement at a single  $Q^2$  value? This is well known to be impossible for electron scattering. However, we make the reasonable assumptions that:

1. The normalized neutron and proton densities are approximately the same.
2. The difference is described to first order in  $R_n$ .

At our value of  $Q^2$ , we are predominantly sensitive to  $R_n$  and only slightly sensitive to other shape parameters. Thus it would take a drastic difference in shape between the proton and neutron densities which is well outside the present theories to cloud the interpretation.

We emphasize that the sensitivity to the shape dependence of the neutron density is not a problem for comparing to theory. We are measuring a well-defined form factor of the neutron density at this  $Q^2$ . Theoretical models can simply calculate this form factor for a direct comparison with experiment.

## III CHOICE OF NUCLEUS AND KINEMATICS

There are two nuclei that are attractive for our measurement, Pb and Ba. They are both equally accessible experimentally. Pb has two main advantages: 1) It is very well known and has a simple structure; and 2) It has the largest

separation to the first excited state (2.6 MeV) of any heavy nucleus, thus lending itself to a flux integration detection technique. Ba has the advantage that it is one of the nuclei being used for an atomic physics test of the Standard Model. A Pb measurement will greatly constrain the effective interactions used in mean field theories and significantly reduce the theoretical spread in  $R_n$  predictions for Ba or many other nuclei. This is illustrated in Fig. 2 by the two theories being approximately parallel lines as a function of  $A$ .

The choice of kinematics is guided by the objective of minimizing the running time required for a 1% accuracy in  $R_n$ . Figure 3 shows for the case of  $^{208}\text{Pb}$  the three ingredients which enter into this optimization: the cross section  $d\sigma/d\Omega$ , the parity violating asymmetry  $A$ , and the sensitivity to the neutron radius  $\epsilon = dA/A = (A1 - A)/A$  where  $A$  is the asymmetry computed from a mean field theory (MFT) calculation [3] and  $A1$  is the asymmetry for the MFT calculation in which the neutron radius is increased by 1%. These three ingredients, which each vary with energy and angle, are plotted in figure 3 for a beam energy of 0.85 GeV which turns out to be the most feasible energy. The optimal kinematics can be determined from the allowable settings for angle and momentum of the spectrometers by searching for the minimum running time, which is equivalent to maximizing the product

$$\text{FOM} \times \epsilon^2 = R \times A^2 \times \epsilon^2$$

where  $R$  is the detected rate and is proportional to  $d\sigma/d\Omega$ , and ‘‘FOM’’ is the conventionally defined figure of merit for parity experiments,  $\text{FOM} = R \times A^2$ . Note that rather than only maximizing the conventional FOM, we take into account the sensitivity ( $\epsilon$ ) to  $R_n$  which varies with kinematics.

The optimization calculations take into account the averaging over the finite acceptance and the energy resolution needed to discriminate inelastic levels. Figure 3 shows the product  $\text{FOM} \times \epsilon^2$  for  $^{208}\text{Pb}$  which peaks at  $E = 0.85$  GeV. The running time  $T$  in days to reach a 1% accuracy in  $R_n$  is approximately  $T \approx 7/(P^2 I \Omega)$  days, where  $P$  is the polarization,  $I$  is the average beam current in  $\mu\text{A}$  and  $\Omega$  is the solid angle acceptance of the spectrometer in steradians. This optimum point corresponds to  $q = 0.45 \text{ fm}^{-1}$ . As an aside, we mention that in the plots of  $\text{FOM} \times \epsilon^2$  one can see a secondary ridge where one might want to perform a second measurement at higher  $Q^2$  to check the shape dependence; the experimental running time becomes longer for a given accuracy, but the required accuracy can be reduced.

## IV APPARATUS

### A Overview

This experiment is proposed for a beam energy of 850 MeV and a  $6^\circ$  scattering angle. The two identical 3.7 msr spectrometer systems consisting

of the Hall A septum magnets plus HRS spectrometers will focus elastically scattered electrons onto total-absorption detectors in their focal planes. A  $50\mu\text{A}$ , 80% polarized beam with a 30 Hz helicity reversal will scatter from a foil of lead which is sandwiched between sheets of diamond to improve the thermal characteristics. Ratios of detected flux to beam current integrated in the helicity period are formed, and the parity-violating asymmetry in these ratios computed from the helicity-correlated difference divided by the sum:  $A = (\sigma_R - \sigma_L) / (\sigma_R + \sigma_L)$ , where  $\sigma_{R(L)}$  is the ratio for right(*R*) an left(*L*) handed electrons. Many of the experimental techniques are used by HAPPEX [12] and HAPPEX II [14]. Separate studies at lower rates are needed to measure backgrounds, acceptance, and  $Q^2$ . Polarization is measured once a day by the Møller polarimeter, and monitored continuously with the Compton polarimeter.

## B Polarized Beam

Polarized electrons are produced by photoemission from a strained GaAs crystal. The laser light is polarized by a Pockels cell providing voltage controlled optical phase retardation that is reversed at 30 Hz. The helicity is structured into pairs of 33.3 msec periods of opposite helicity, where the sign of the first in the pair is determined pseudorandomly. Experience has shown that most of the helicity correlations in the electron beam originate from control of the laser light. This is discussed in section V.A.

## C Target Design

Considerations of the target design involves the following factors.

1. Optimizing the thickness and geometry of the target.
2. Improving the thermal properties of the target, which is necessary since lead has a low melting temperature.
3. Boundary radiation in the hall.
4. Influence of the inelastic states.
5. When using a “cooling agent” to improve the thermal properties of the target, which in our design is a diamond film backing (pure  $^{12}\text{C}$ ), we must compute the influence of this agent on the measurement.

As explained below, if the target is a single foil, a thickness of  $\approx 10\%$  of a radiation length (RL) gives the maximum detected rate in our detector, where the upper limit is determined by radiative losses. For running a target this thick, one must also consider the radiation produced in the hall – both the

instantaneous and the integrated radiation. Calculations [16] show a boundary dose of about 2.2 mrem which is 22% of the annual design goal limit. The instantaneous dose, however, is 3 times higher than the allowed average dose rate, and we may want to reduce this with local shielding if the anticipated dose from other experiments running that year is high. A target much thicker than 10% RL therefore seems impractical.

Concerning radiative corrections, we note that they mainly have the effect of reducing our rate by kicking electrons out of the focal plane detector. Otherwise, radiative corrections are not a significant source of systematic error for the experiment because the spectrometer resolution is better than 1% and the electroweak radiative corrections can be calculated reliably at this level.

The maximum “effective” thickness of the target is determined from the energy loss cut imposed by the detector in the focal plane and the Brehmsstrahlung radiative losses in the target. The effective thickness is defined as the product of the actual thickness times the fraction of elastic events detected. The effective thickness is a maximum for an actual thickness of  $\approx 10\%$  RL. In figure 5 we show how the effective thickness varies with the energy cut and with the actual thickness. With a cut at 4 MeV, we can get an effective thickness of 3.7% RL.

By integrating the rate up to 4 MeV, we reduce the running time by 25% at the expense of integrating inelastic scattering which constitutes a fraction 0.5% of our signal. This is a tolerable compromise; see section V.F. on this systematic error contribution. Isotopically separated  $^{208}\text{Pb}$  will be deployed which is 99.1% pure 208 isotope, and the remaining isotopes are 207, 206, and 204 in abundance 0.7, 0.2, and 0.02%.

The power dissipated in the  $^{208}\text{Pb}$  target is 40 Watts for a 50  $\mu\text{A}$  beam. Our target design for improving the heat capacity is shown in figure 6 and includes the following ingredients.

1. A 0.5 mm foil of lead is sandwiched between two 0.2 mm sheets of diamond. Diamond, which is pure  $^{12}\text{C}$ , has several advantages: 1) It has an extremely high thermal conductivity; 2) Since it is a light nucleus it contributes only 6% to our detected rate (note that it cannot be kinematically separated at our low  $Q^2$ ); 3) At our low  $Q^2$  the parity violating asymmetry for  $^{12}\text{C}$  is known to sufficient accuracy ( $\leq 5\%$ ); therefore, since it is a small contaminant the systematic error is negligible. (See also section V.F.)
2. The lead / diamond sandwich will be deployed on the existing solid target ladder of the Hall A cryotarget. It can be easily inserted and retracted from the beam. This installation has virtually no impact on the Hall A program.
3. The existing solid target ladder is being modified to carry cryogenic helium to the solid target assembly. Liquid helium will flow around the

edges of the lead target. This cooling together with the diamond backing will make the target stable up to 100  $\mu\text{A}$  of rastered beam current which provides a factor of 2 safety.

A prototype lead / diamond target will be deployed for tests during the January 2000 shutdown. Some tests were done during 1999 of a prototype lead / aluminum sandwich target. Aluminum foils were used instead of diamond, and the solid target did *not* have liquid helium cooling at its edges, but was in thermal contact with the cryotarget. In these tests the lead target withstood 25  $\mu\text{A}$  for an hour and did not melt. The new liquid helium cooled lead / diamond target is a superior design and calculations show it will withstand 100  $\mu\text{A}$ .

## D Spectrometer and Detector

The septum magnets being built by the INFN group [11] will extend the angular range of the HRS down to  $6^\circ$ . Monte Carlo simulations show a solid angle acceptance of 3.7 msr per spectrometer. During running of the early septum magnet experiments, we will study issues of acceptance, backgrounds, and the systematics of  $Q^2$ . Some brief facility development runs can be performed with the lead target.

The distribution of rates and asymmetries in the focal plane are shown in figure 4. The first excited state of  $^{208}\text{Pb}$  is at 2.6 MeV and could be discriminated by the high resolution of the spectrometers, but we will instead choose to integrate up to 4 MeV to catch a good fraction of the radiative tail and increase the rate. (See section V.F. for a discussion of the correction due to the excited states.) The rates are high, 860 MHz in each spectrometer. A total absorption detector made of quartz-lead sandwich will be constructed to integrate the elastically scattered electrons. The signal in each helicity window will be integrated.

The detector will be similar to the HAPPEX detector, which was a sandwich of lead and lucite. One important difference for the present detector is that the radiation levels are higher, and we are concerned that the lucite will turn yellow and degrade the performance. Hence we plan to use amorphous silicon or “quartz” as the radiating element. An important advantage of the present experiment is that the detector is much smaller, which will keep the costs down.

One possible technology is the use of quartz fibers. They can be obtained as thick as 880 microns and cost \$20/m in bulk. The detector would have about 10 layers of fibers between 1 radiation length sheets of lead. A schematic diagram, showing only 6 layers, is given in figure 7. Due to the simple geometry, an air lightguide is sufficient to transport the light to the phototube as shown. Another possibility is to use quartz plates. Since the

**TABLE 2.** Acceptance Averaged Rate and Asymmetry

Measured Asymmetry ( $p_e A$ )	0.51 ppm
Beam Energy	850 MeV
Beam Current	$50\mu A$
Required Statistical Accuracy	3%
Energy Cut (due to detector)	4 MeV
Detected Rate (ea spectrometer)	860 MHz
Running Time	680 hours

detector is small, light collection is no problem. We will investigate this possibility. The detector will be easy to install in the focal plane above the VDC drift chambers. The rate in the spectrometer hut should not harm the other detectors, which will be turned off.

Table 2 shows the rates, asymmetries, and running times.

## V SYSTEMATICS

Measuring a tiny asymmetry of 0.5 ppm to 3% absolute accuracy is a major challenge involving the following considerations which will be discussed in this section.

1. The experimental systematic error must be much smaller than the statistical goal ( $1.5 \times 10^{-8}$ ), hence a goal of  $\leq 10^{-9}$ . The main issues here are with the control of false asymmetries associated with helicity correlated beam parameters such as intensity, energy, and position. We discuss below the development plan to address this issue, and the experience from HAPPEX.
2. Because of the high rates (860 MHz per spectrometer), the statistical error in each 30 msec window will be 140 ppm. All other noises, e.g. instrumental noises, must be kept well below this.
3. The normalization of the asymmetry must be better than 3%. There are two main issues: the  $Q^2$  measurement and the beam polarization. We expect to be able to measure  $Q^2$  to 0.3%. Our goal for the polarization measurements is 1%.
4. Since we must integrate our detected signal, the backgrounds must be measured separately; in addition, pedestals and nonlinearities need to be controlled at the few tenths of percent level.
5. Several theoretical issues have recently been addressed [15] and we will mention them briefly in this section. These include corrections due to

Coulomb distortions, dispersion corrections, meson exchange currents, shape dependence, inelastic contributions, isospin violations, and target impurities. In addition the relationship to atomic parity violation experiments has been studied in more detail recently by Pollock [15].

## A Helicity Correlated Beam Parameters

In the past year, a great deal has been learned about running with strained GaAs photocathodes at Jefferson Lab. Because the strain introduces an optically active axis, helicity correlated variations in the laser beam's polarization state and direction have a pronounced effect on parameters of the accelerated beam such as position. Techniques have been developed to reduce the helicity correlated beam positions in the injector by minimizing the sensitivity of the laser optics to changes associated with the Pockel Cell used to produce polarized light. These developments will continue in collaboration with the polarized injector group, G0 experiment, and HAPPEX II experiment.

During HAPPEX, the correction due to beam parameters was  $3 \pm 3 \times 10^{-8}$ . These were negligible for HAPPEX but we want to reduce this systematic error by a factor of  $\approx 10$  for this proposal. There are two aspects to this problem: 1) The helicity-correlated position differences, which affects the correction; and 2) The accuracy of the beam position measurements, which affects the error in the correction.

The position correlations for the strained GaAs running for HAPPEX were larger than desired. The main reason was that the beam tune had unnecessarily large beta functions. This tune resulted from a need to have a tight beam in the Compton polarimeter together with a lack of appropriate quadrupoles in the Hall A beam line. With the new quadrupoles anticipated for the 2000 January shutdown, we should be able to develop ideal tunes which will eliminate the helicity correlated position differences on target. In addition, new controls of systematics are being developed for the polarized source. We believe we can solve the position correlation problem, making the corrections at most comparable to the statistical error.

The error in the position corrections was due to  $20\mu\text{m}$  position jitter in the beam at the target. However the true noise is the electronic position monitor noise. One of our monitors showed  $0.8\mu\text{m}$  noise, presumably due to the small beta function at that point. This provides a measure of the intrinsic monitor noise which is 25 times smaller than the value used to compute the HAPPEX error, or  $1 \times 10^{-9}$ . This will be adequate for the present proposal if the sensitivities are no worse than for HAPPEX. We will need some beam studies with the lead target to measure these sensitivities, study the monitor noise, and see where we stand. A possible upgrade is to use cavity position monitors developed for G0.

## B Fluctuations in the Asymmetry

Integrating a total of 1.7 GHz leads to a counting statistic error of 140 ppm in each 30 msec helicity window. In order to have our error dominated by counting statistics all other sources of noise must be much smaller than this. Again the HAPPEX experiment can be used as an indication of the magnitude of the problems we may encounter, though we expect that by the time we run this proposed experiment several improvements are possible. The following contributions to noise in HAPPEX are relevant. 1) Electronic noise of beam current monitors, 30 ppm; 2) Electronic jitter in the detected flux contributed 100 ppm, but this was caused mainly by long cable runs to our ADCs – if we place the DAQ crates in the shield huts near the detectors this error should go down to about 30 ppm; and 3) Beam jitter of about 20 microns corresponding to 20 ppm in the asymmetry (for the LH2 target).

These and other noises can be studied during engineering runs with the lead target prior to the experiment. A further source of noise we expect is from rastering the beam. This fluctuates the cross section by about 1%. Estimates show that this should cancel between helicity pairs because of the fast repetition of raster orbits.

## C Normalization Errors - $Q^2$ and Polarization

The two main normalization errors are  $Q^2$  measurement and beam polarization. Since the beam energy and the scattered momentum can each be measured to better than 0.1%, we expect to measure  $Q^2$  for elastic scattering to 0.1%. We can make a cross check using the scattering angle, for which a systematic error of 0.3 mrad from a careful survey is achievable. The asymmetry is approximately proportional to  $Q^2$  and it should therefore be possible to keep this systematic error  $\leq 0.3\%$ .

Accurate beam polarimetry is important for the future of Jefferson Lab. Polarization is measured with a Mott polarimeter at the 5 MeV region of the accelerator, with a Møller polarimeter in Hall A, and with a Compton polarimeter in the Hall A beamline. As a standalone device, the Møller polarimeter is presently capable of a 3.2% accuracy in the polarization. In the future, 2% is projected, the limit being the target foil polarization systematics.

We plan to measure the polarization once a day using the Møller polarimeter. We will try to use the Compton polarimeter to monitor the polarization online between Møller measurements. At 850 MeV the statistical accuracy of the Compton is significantly worse than at higher energies but should be sufficient for one 1% measurements in 16 hours (statistical error only). At present the Compton polarimeter has a systematic error in the absolute polarization of 4.3% at 3.3 GeV. In the future, 2% error is the expected to be possible at 3.3 GeV. The systematics at 850 MeV are much different and may

be worse than at high energies, but we can use the Compton polarimeter at high energies for cross calibrating Møller. Since the limiting error in the Hall A Møller polarimeter is the target polarization, this cross calibration essentially calibrates the target polarization.

We note that continuous monitoring at 850 MeV is not critical for this experiment; the preliminary results of online Compton measurements during HAPPEX have shown that the beam polarization is stable between Møller measurements if nothing significant is changed at the polarized source such as a re-ciesation.

The Mott polarimeter and Hall C Møller polarimeter provide useful cross checks. The Hall C Møller polarimeter has reduced the systematic error in their target foil polarization by saturating the foil in a high field. A systematic error of  $\approx 0.5\%$  has been claimed.

It will be a challenge to reduce the polarization error to the 1% level that we want for this proposal. At present, 2% seems within reach by the time we run, but improvements in target foil systematics could push this to the 1% level. We note that the difference between a 1% and 2% polarization error is an increase in our total experimental error from 3.2% to 3.6%.

## D Backgrounds

Separate measurements at low rates, as well as Monte Carlo studies, need to be performed to understand the backgrounds. Such studies have been done for the HRS spectrometers [17] and need to be repeated for the septum magnet setup. Early data from running the septum magnet can also be used to study backgrounds. The relevant results from the HRS study and the implications for this proposal are:

1. Inelastically scattered electrons, or those from the radiative tail, can rebound inside the spectrometer and strike the detector. The inelastics were a 0.2% contribution during HAPPEX and should be less of a problem for this proposal because the ratio of inelastic to elastic is very small.
2. Some electrons may scatter from the magnetized iron in the spectrometer and strike the detector. This is a potentially serious problem because Møller scattering from polarized electrons in the iron creates an asymmetry. For the HAPPEX setup pole-tip scattering was measured to be a  $\leq 10^{-5}$  contribution to our detected flux implying  $\leq 10^{-9}$  to the asymmetry. Simulations confirmed this. For the present proposal it should be an even smaller problem because the septum magnet collimates more strictly the trajectories that come near pole tip faces. Lower energy electrons that rebound in the spectrometer do not see the pole tips.
3. Inelastic states and target impurities are a negligible systematic (see section V.F).

## E Pedestals and Nonlinearity

During HAPPEX we found that measuring pedestals once a day reduces the error in them to 0.1% while their drift was 1% over a 1 day period. Non-linearities can be measured once per day to 0.1% and are probably stable at the 0.2% level. The effect of pedestal errors or nonlinearity is to produce a systematic which is approximately the product of the error times the largest asymmetry in the devices they affect. For example, a 0.1 ppm beam current monitor asymmetry with a 1% nonlinearity produces a  $\approx 1 \times 10^{-9}$  systematic. If we run with adequately low noise in the beam parameters similar to what was observed during HAPPEX, and if we achieve the aforementioned pedestal errors and nonlinearities, the effects on this proposal will be acceptable.

## F Theoretical Corrections

A manuscript that describes the theoretical corrections to the asymmetry and the relevance to atomic parity violation experiments is being prepared for publication [15]. We will briefly summarize the results here.

1. Coulomb distortions are the largest known correction to the asymmetry, about 20% for the  $^{208}\text{Pb}$ , and have been accurately calculated in a relativistic optical model by Horowitz [3]. This was also discussed in section II.E.
2. The sensitivity to the strangeness radius was estimated to be less than 1%. This estimate used the published HAPPEX [12] and SAMPLE [13] results and assumed a standard dipole form factor for strangeness. Better limits on the strangeness radius (static moment) should be obtained by HAPPEX II prior to the experiment proposed here.
3. Parity admixture contributions to the asymmetry are negligible because the initial and final state are spin zero, a single  $0^+$  multipole operator contributes in Born approximation, thus supporting no parity violating interference [15] [18].
4. Meson exchange currents were estimated to change the weak radius we measure by  $r_{\text{MEC}}^2/R_n$  where  $r_{\text{MEC}}^2$  is the square of the average distance weak charge is moved by MEC and  $R_n$  is the neutron radius. This ratio is small.
5. Dispersion corrections are of order  $\alpha/Z$  which is negligible.
6. There has been some concern about the shape dependence and the meaning of what we are measuring, which is not exactly  $R_n$ . Instead we are measuring the neutron form factor at a small  $Q^2$ . There is no problem with comparing to nuclear theory since these theories must compute the

**TABLE 3.** Error Budget

Source of Error	$\frac{\Delta A}{A}$ (%)
Polarization	1.0 (2.0)
$Q^2$ Determination	0.3
Finite Acceptance	0.3
Beam Systematics	0.2
Backgrounds	0.2
Total Systematic Error	1.1 (2.1)
Statistics	3.0
Total Experimental Error	3.2 (3.6)

form factor, and there isn't any need to extract a neutron radius. Our measurement will be a good first step at calibrating theory as illustrated in figure 2. This point was discussed in section II.E.

7. The application of our measurements to atomic parity violation is fairly direct because to a good approximation the shape dependence enters the atomic variables the same way it enters our electron scattering asymmetry as demonstrated by Pollock [15].
8. We accept inelastic contributions up to 4 MeV, which are 0.5% of our signal. The main contribution is the first excited state at 2.6 MeV. The asymmetry from this state was estimated to be  $1.25 \pm 0.25$  times the elastic asymmetry.
9. Calculations of isospin violations in the nucleon [4] suggest only small corrections. Isospin symmetry is not assumed for the nucleus; instead, a formalism is used which treats the proton and neutron densities independently.
10. The impurity from the diamond backing should be a negligible systematic. The asymmetry for  $^{12}\text{C}$  has been computed with sufficient accuracy [3], including Coulomb distortions. Isotopic impurities in the target (0.9%, mostly 207 and 206 isotopes) are unimportant.

## G Error Budget

The experimental errors which we will need to achieve are given in table 3. We note that if the polarization error were limited to 2% the total experimental error would be 3.6% instead of 3.2%.

## VI BEAM TIME REQUEST

We request 720 hours of running or 30 days. The breakdown is: 1) 680 hours to achieve 3% statistical accuracy with  $50\mu\text{A}$  of 80% polarized beam. 2) A one hour Møller polarimeter measurement once per 24 hours of beam-on-target, hence a total of 30 hours for Møller. 3) 10 hours for setup and checkout of the detector alignment and auxiliary measurements of  $Q^2$  and backgrounds.

We plan to study the systematics of the strained GaAs polarized beam parasitically; this work was already begun in 1999 and will continue as preparation for HAPPEX II and G0. If successful, these beam studies will demonstrate that the beam and beam line instrumentation are adequate.

We will participate in the commissioning of the septum magnet and will use data from that commissioning as well as early experiments to examine issues of acceptance, backgrounds, and systematics of  $Q^2$ . Prior to our production run, we'll need to set up the septum magnet. Some facility development time will be needed to verify that our target and detector works and has good noise characteristics.

## REFERENCES

1. H. de Vries, C. W. de Jager, C. de Vries, Atomic and Nuclear Data Tables, **36**, 495 (1987).
2. T.W. Donnelly, J. Dubach, and I. Sick, Nucl. Phys. **A503**, 589 (1989).
3. C. J. Horowitz, Phys. Rev. C **57**, 3430 (1998).
4. S.J. Pollock, E.N. Fortson, and L. Wilets Phys. Rev. C **46**, 2587 (1992).
5. E.N. Fortson, Y. Pang, and L. Wilets, Phys. Rev. Lett. **65**, 2857 (1990).
6. L. Ray and G.W. Hoffmann, Phys. Rev. C **31**, 538 (1985).
7. C. Olmer *et al.*, Phys. Rev. C **21**, 254 (1980).
8. C.J. Horowitz, private communication.
9. P. Ring *et al.* Nucl. Phys. A **624**, 349 (1997).
10. Relativistic Optical Code RUNT, E.D. Cooper private communication, D. Vretenar *et al.*, Los Alamos preprint nucl-th/9911024, and B.C. Clark *et al.* private communication.
11. "A Proposal for Two Septum Magnets for Forward Angle Physics in Hall A at TJNAF", Submitted to the TJNAF Technical Advisory Committee, Hypernuclear Collaboration (1996).
12. K. A. Aniol *et al.*, Phys. Rev. Lett. **82**, 1096 (1999).
13. B. Mueller *et al.*, Phys. Rev. Lett. **78**, 3824 (1997).
14. Jefferson Lab proposal PR-99115, "Constraining the Nucleon Strangeness Radius in Parity Violating Electron Scattering", accepted by PAC16.
15. "Parity Violating Measurements of Neutron Densities", C. J. Horowitz, S. J. Pollock, P. A. Souder, R. Michaels, manuscript soon to be submitted to Los

Alomos nucl-th/9912???, and available as postscript file at [www.jlab.org/~rom/NeutronDensity.ps](http://www.jlab.org/~rom/NeutronDensity.ps)

16. P. Degtiarenko, memo on radiation budget.
17. “Empirical Study of Backgrounds for HAPPEX in Elastic Electron–Proton Scattering” R. Michaels, unpublished technical report (1998).
18. T.W. Donnelly, private communication.
19. C. Cothran, memo on solid target heating.
20. P.A. Souder *et al.*, Phys. Rev. Lett. **65**, 694 (1990).

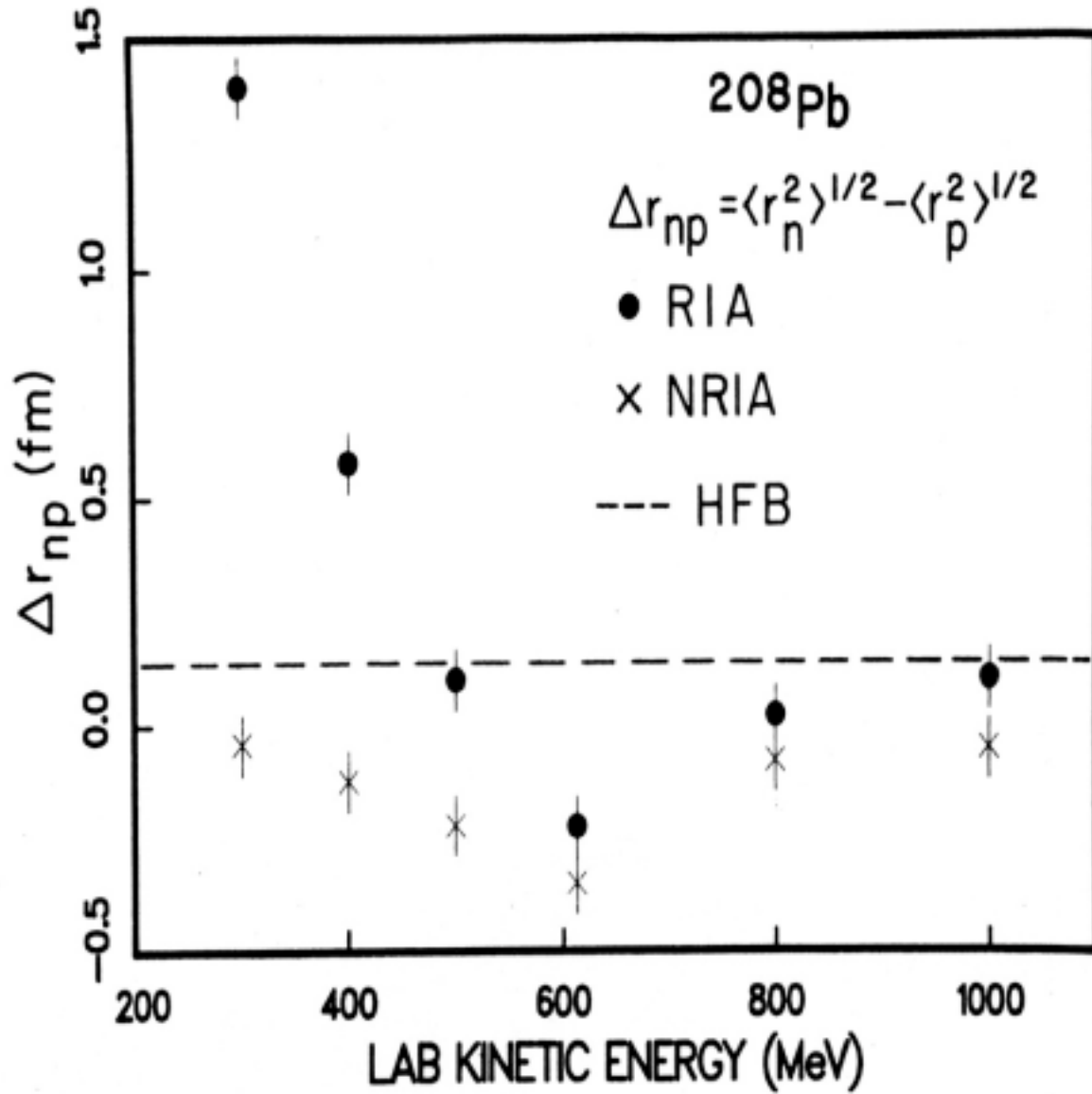
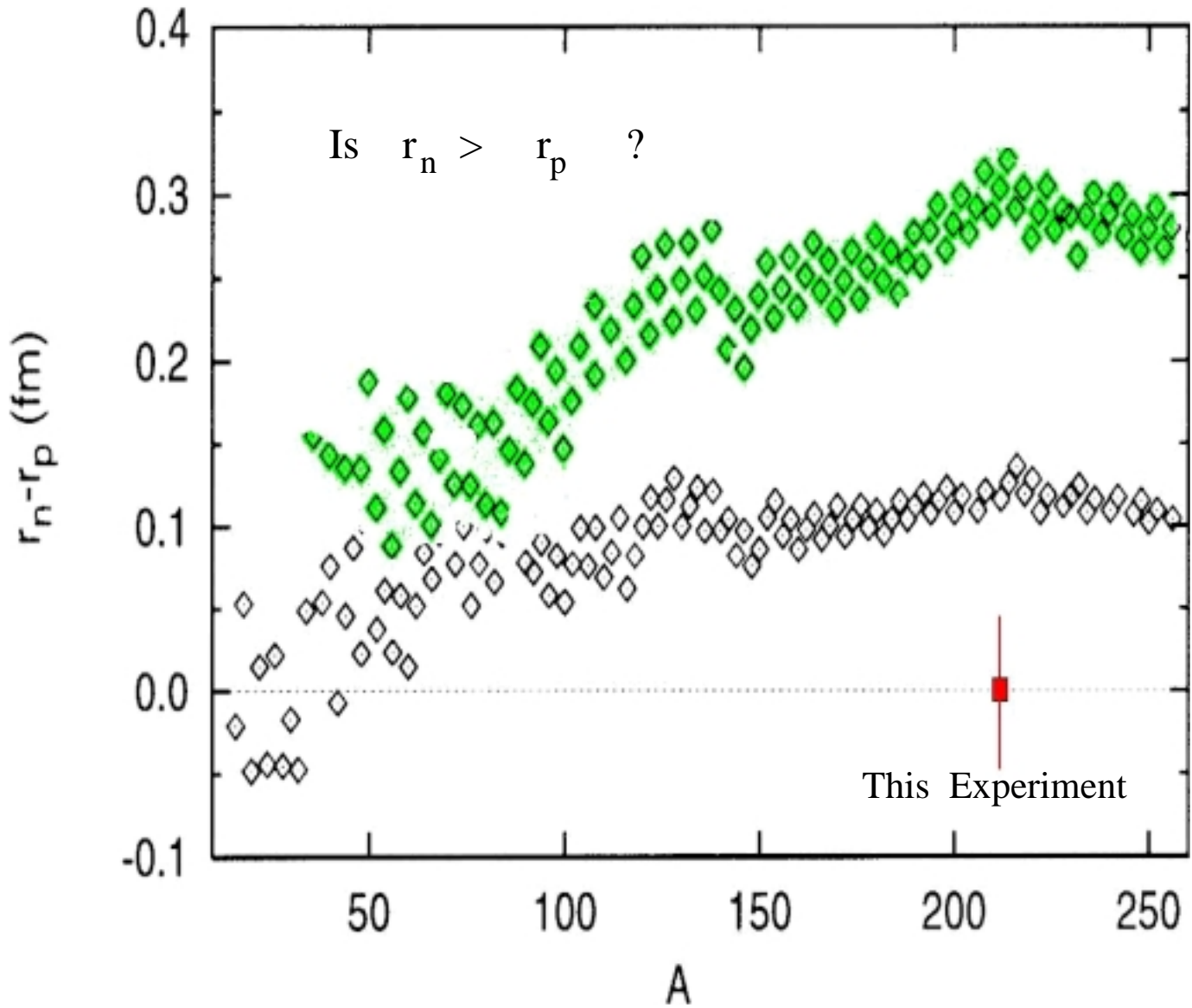
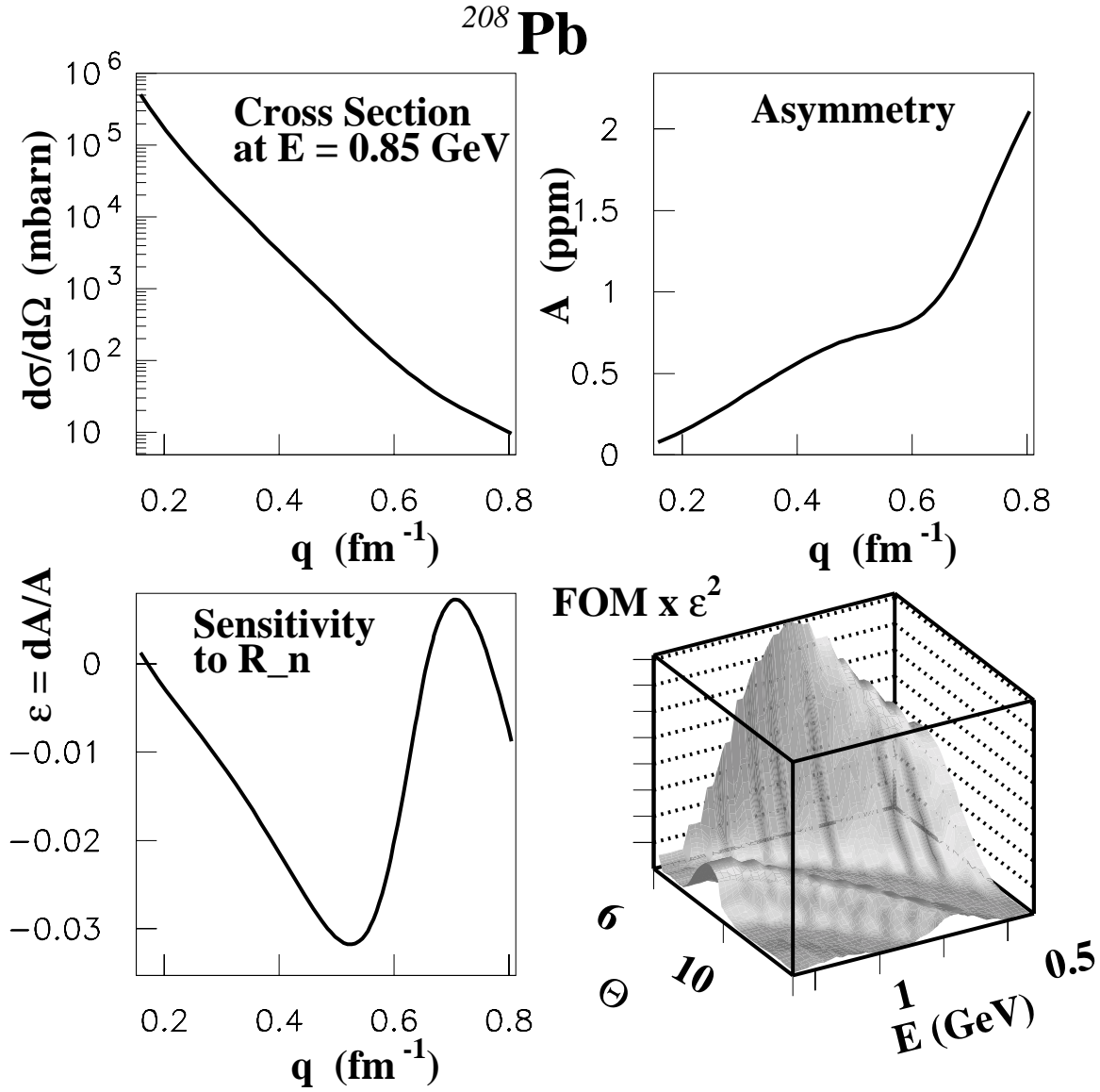


FIGURE 1. Neutron-proton RMS radii differences for  $^{208}\text{Pb}$  deduced from proton nucleus elastic scattering using RIA (solid dots) and the first order NRIA (crosses). The theoretical Hartree-Fock-Bogoliubov (HFB) value is indicated by the dashed line. This figure is taken from reference 6 where it is called fig. 10.



**FIGURE 2.** Difference between neutron radius and proton radius for two mean field theories versus atomic number  $A$ . Also shown is the projected error bar of this experiment. Calculations are from reference 9.



**FIGURE 3.** Cross section, parity violating asymmetry, and sensitivity to  $R_n$  for  $^{208}\text{Pb}$  elastic scattering at 0.85 GeV. The fourth plot shows the variation of  $\text{FOM} \times \epsilon^2$  with energy and angle, showing an optimum at 0.85 GeV for a  $6^\circ$  scattering angle which corresponds to  $Q = 0.45 \text{ f}^{-1}$ .

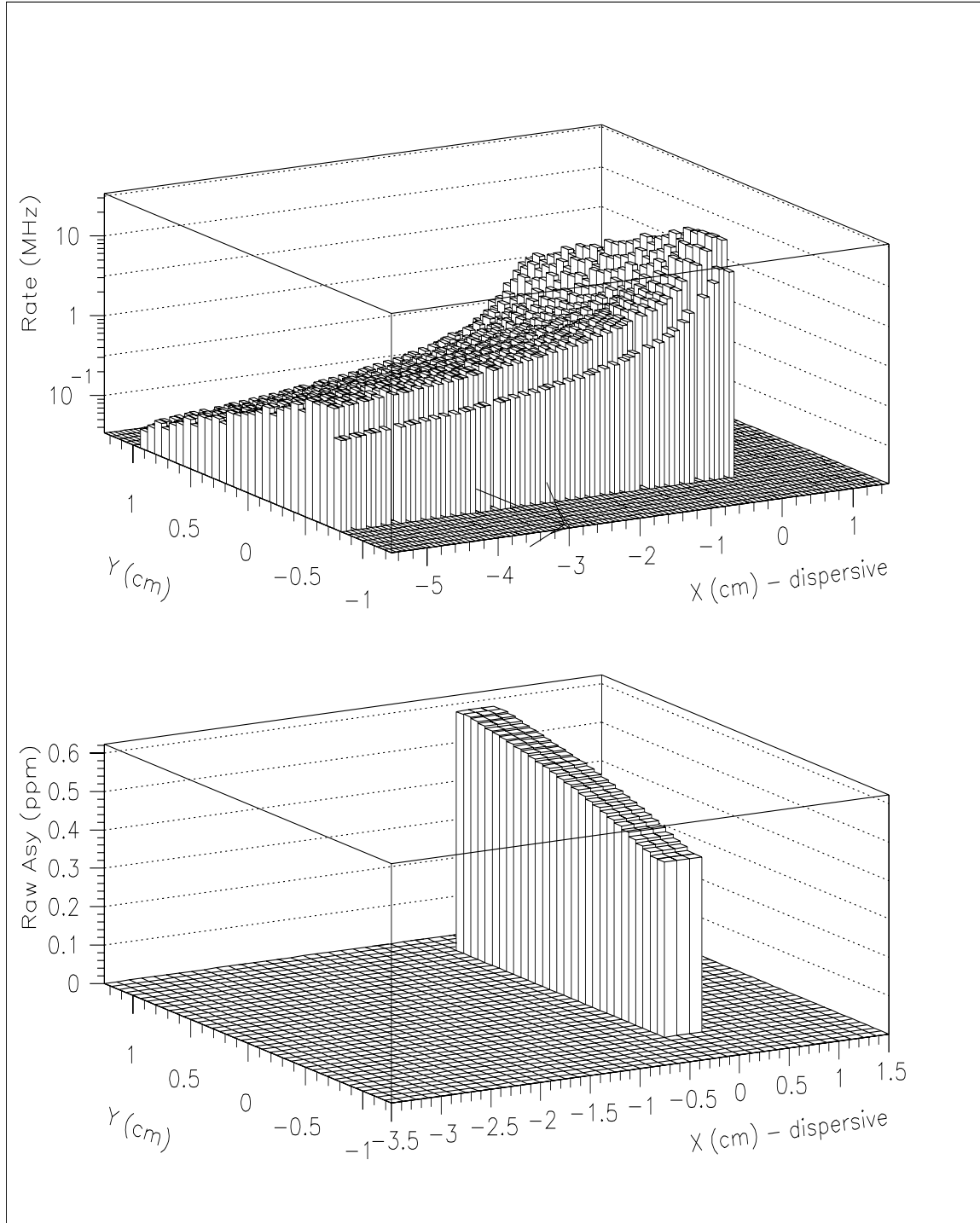


**FIGURE 4.** The two plots are: a) top: Scattering rate as a function of X-Y position in focal plane. b) bottom: Unradiated raw asymmetry (product of polarization times asymmetry) versus X-Y. Note the different scale in X. The radiative tail, shown in the top figure, extends towards -X. The location of 2 MeV separation from the elastic peak is shown by the arrow at -3 cm in the top figure.

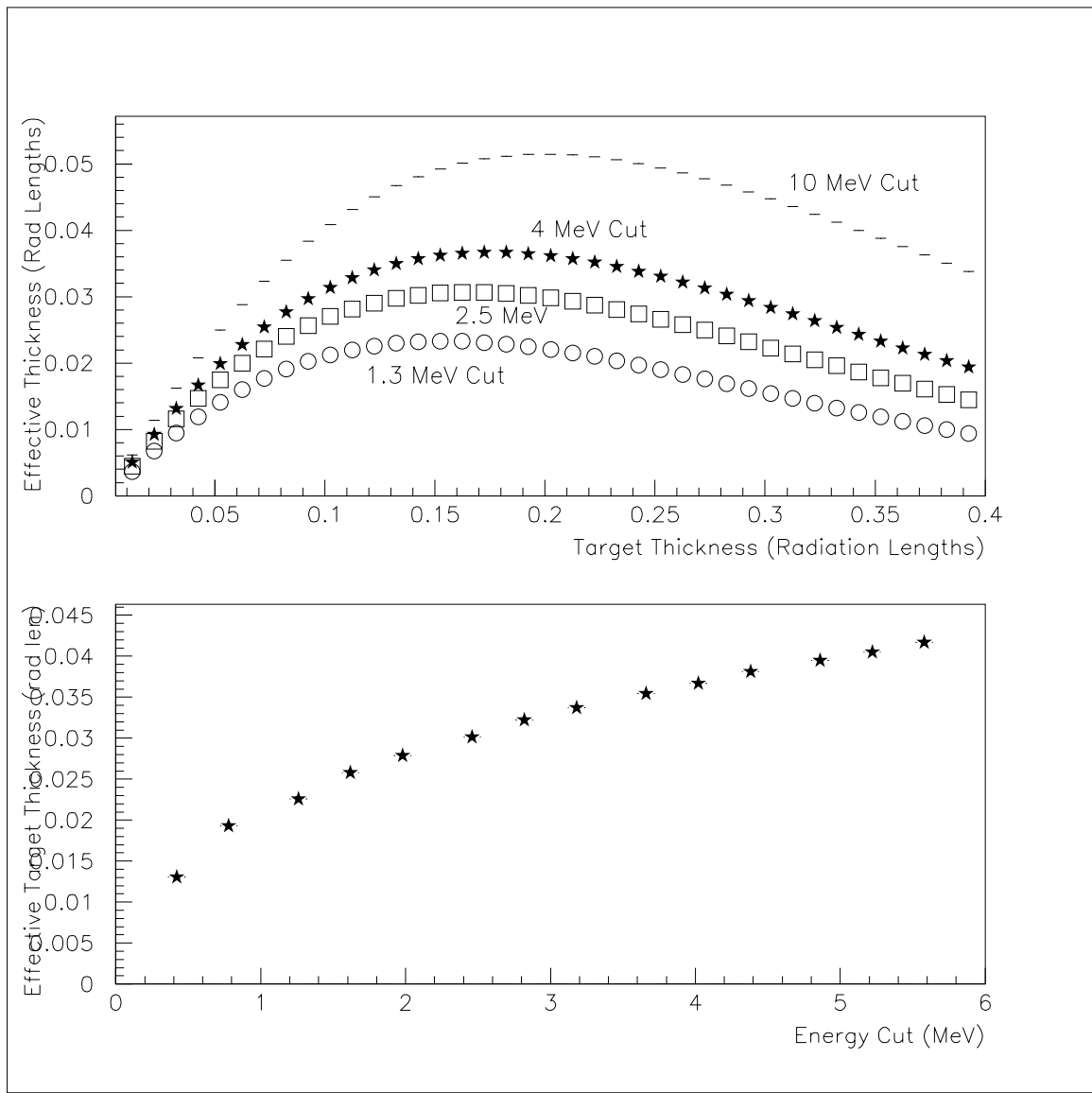


**FIGURE 5.** Effective target thickness, defined as the product of the actual target thickness times the fraction of events that go into the detector. Top figure: Effective thickness as a function of the actual thickness for various energy cuts imposed by the detector. Bottom figure: The maximum effective thickness as function of the energy cut.

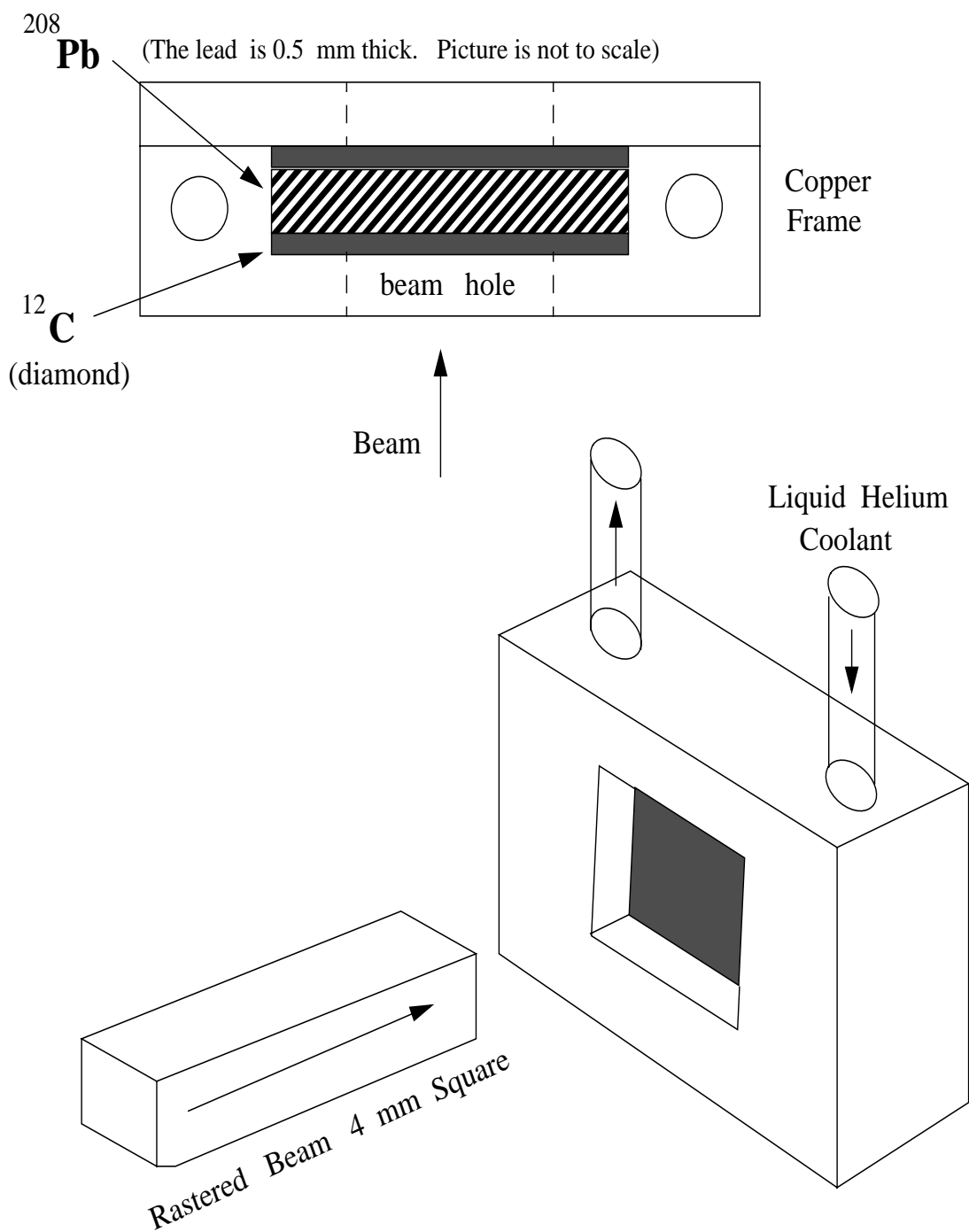


**FIGURE 6.** Conceptual sketch for the lead / diamond target. The 0.5 mm thick lead foil is sandwiched between 0.2 mm thick sheets of diamond which has a very high thermal conductivity. Liquid helium flows around the boundary of the target. The assembly is clamped with spring-like washers that take out slack due to differential thermal expansion.

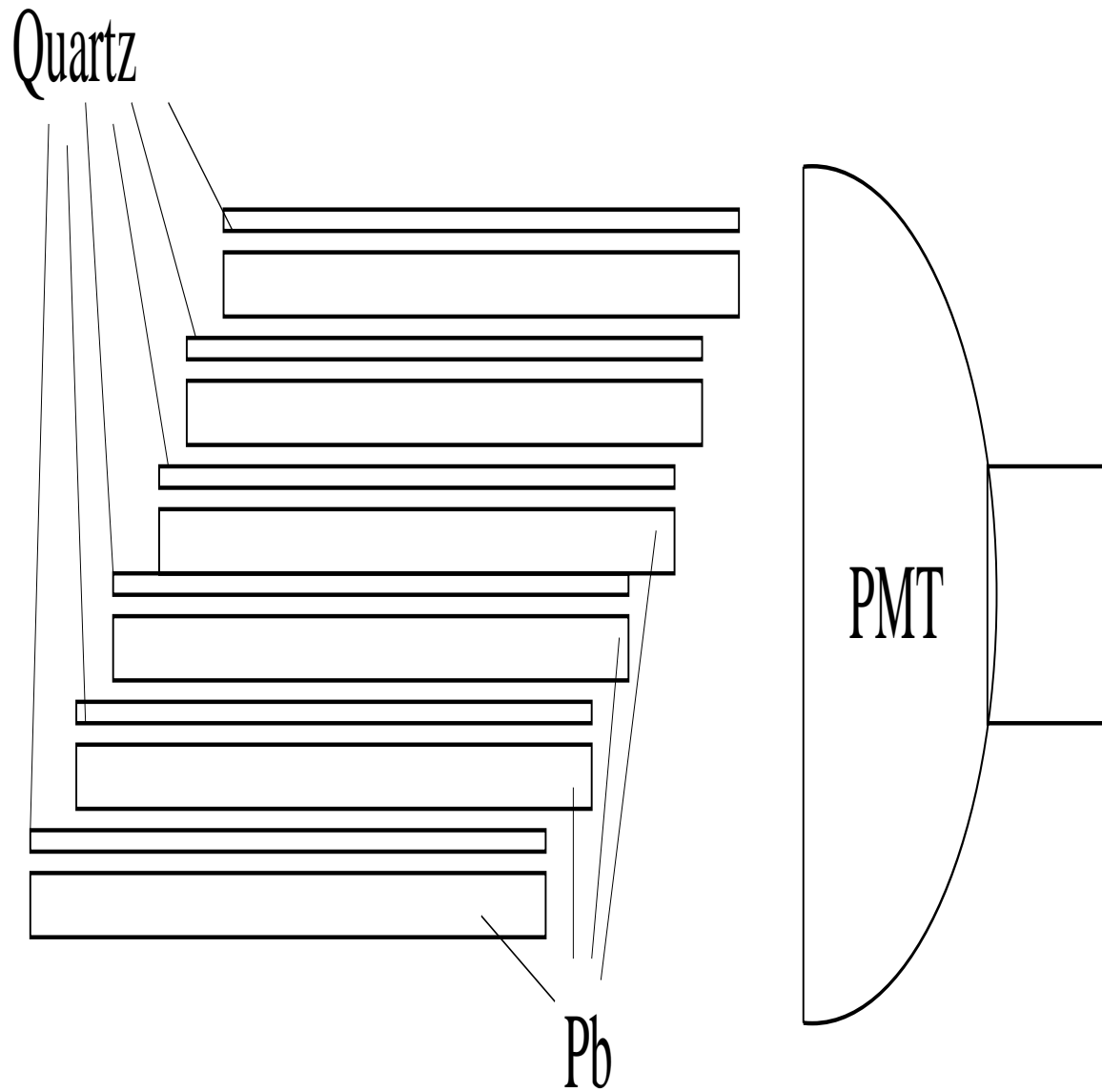


**FIGURE 7.** Detector for the Spectrometer Focal Plane. A stack of lead and quartz integrate electrons in a small area of approximately 5 cm by 5 cm where they are focussed.